The Effects of C_{bc} on the Linearity of AlGaAs/GaAs Power HBTs

Woonyun Kim, *Member, IEEE*, Sanghoon Kang, Kyungho Lee, Minchul Chung, Youngoo Yang, *Student Member, IEEE*, and Bumman Kim, *Senior Member, IEEE*

***Abstract*—It is well known that C_{bc} is the dominant nonlinear element in heterojunction bipolar transistors (HBTs). To study its behavior, an analytical nonlinear HBT equivalent-circuit model has been developed. The present model includes the effect of the ionized donor charge in the depleted collector region compensated by the injected mobile charge. The model-based simulation shows that, at a small-signal range, the third-order intermodulation (IM3) of the normal HBT has the normal 3 : 1 gain slope generated by the nonlinearity of C_{bc}. At a large-signal level, the load line passes through some regions with constant C_{bc} because its collector is fully depleted by the injected free carriers, and the growth rate of the IM3 is decreased. The punch-through collector HBT has constant C_{bc} during the whole RF cycle, and the IM3, which is generated by g_m nonlinearity, has the normal 3 : 1 gain slope for the all input signal level. Therefore, the IM3 level is significantly lower for the punch-through HBT at a low-power level, but the IM3s of both devices are comparable at a high-power level. The experiment supports our proposed model.**

***Index Terms*—Base–collector capacitance, heterojunction bipolar transistors, intermodulation distortion, linearity.**

I. Introduction

THE transmitter of the handset of digital mobile communication systems requires highly efficient linear power amplifiers [1]–[4]. Heterojunction bipolar transistors (HBTs) are widely used for the amplifiers and their intermodulation (IM) behavior has been extensively measured and analyzed [4]–[12]. The good linearity of HBTs has been attributed to the partial cancellation of intrinsic nonlinear currents [5], [8], [10] or the feedback effect of the emitter and base resistances [9]. It is commonly known that C_{bc} is the dominant nonlinear source and should be linearized to reduce the IM distortions [7], [9]–[12]. The HBTs with the punch-through collector at the operation bias point showed a higher third-order intermoduation intercept point (IP3) than the normal HBTs. However, the IP3 represents a small-signal behavior only. To investigate the contribution of the nonlinear C_{bc} for the distortion at a large-signal level, we developed an analytical nonlinear HBT model in a commercially available harmonic balance simulator, i.e., ADS, using symbolically defined devices (SDDs). By considering self-heating and recombination effects, the model accurately describes the bias dependence of the current gain.

Manuscript received August 18, 2000. This work was supported in part by the Agency for Defense Development and by the Ministry of Education under the Brain Korea 21 Project.

The authors are with the Department of Electronic and Electrical Engineering and Microwave Application Research Center, Pohang University of Science and Technology, Kyungbuk 790-784, Korea (e-mail: kwn@postech.ac.kr; bmkim@postech.ac.kr).

Publisher Item Identifier S 0018-9480(01)05045-1.

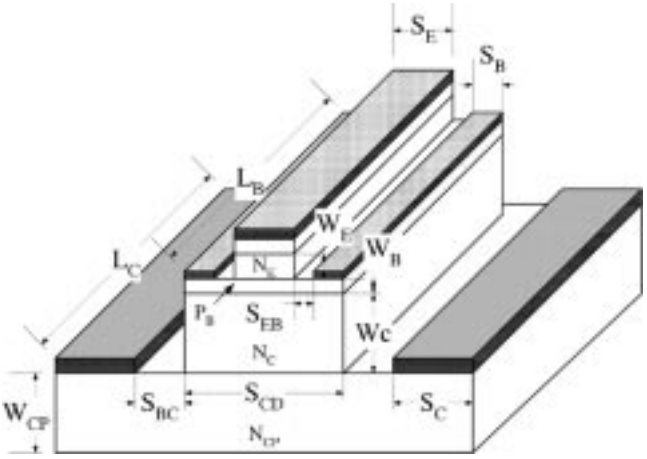

Fig. 1. Schematic of the HBT used for the analysis.

The physically based large-signal HBT model includes the effect of the ionized donor charge in the depleted collector region compensated by the injected mobile charge. The C_{bc} is, therefore, dependent not only on the base–collector voltage, but also the collector current. In order to study the C_{bc} effects on nonlinear properties, we compared two kinds of HBTs. The punch-through HBT has a fully depleted collector by the collector bias voltage even at a low current level. It has constant C_{bc} during the whole RF cycle, and its third-order intermodulation (IM3) has the normal 3 : 1 gain slope for all signal levels. On the other hand, the HBT with the normal collector exhibits a strong nonlinearity of C_{bc} at a small input power, and the IP3 of the HBT is a lot lower than that of the punch-through HBT. At a large-signal level, however, the collector can be fully depleted by the injected charge and C_{be} becomes constant for the some portion of RF cycle. Therefore, the gain slope of the IM3 is decreased and at a very high power level, and IM3 is almost comparable to that of the punch-through HBT. To verify the model, HBTs with a punch-through collector and normal collector were fabricated and tested. The experimental data support the results of the present model.

II. Nonlinear HBT Model

The schematic HBT structure used for the analysis is shown in Fig. 1. In this figure, S_i, L_i, and W_i are the width, length, and thickness for the emitter, base, and collector ($i = E, B,$ and C), respectively. The doping concentrations of the emitter, base, collector, and subcollector are N_E, P_B, N_C, and N_{CP}, respectively, and the distances between the emitter and base and

TABLE I
HBT MODEL PARAMETERS USED IN THE SIMULATION

Symbol	Value	Symbol	Value
ρ_{EC}	$1 \times 10^{-6}\Omega cm^2$	$\epsilon_{E,AlGaAs}$	$1.09 \times 10^{-12}F/cm$
ρ_{BC}	$3 \times 10^{-6}\Omega cm^2$	ϵ_B, ϵ_C	$1.16 \times 10^{-12}F/cm$
ρ_{CC}	$1 \times 10^{-6}\Omega cm^2$	V_{TH}	0.0259 V
L_E	22 μm	ΔE_C	0.205 eV
L_B	26 μm	ΔE_V	0.109 eV
L_C	26 μm	N_{CD}	$4.7 \times 10^{17}cm^{-3}$
S_E	2 μm	N_{VA}	$7.0 \times 10^{18}cm^{-3}$
S_B	1 μm	m_n^*	$0.07m_o$
S_C	3 μm	m_p^*	$0.5m_o$
S_{EB}	0.2 μm	v_{sat}	$4.1 \times 10^7 cm/s$
S_{BC}	3 μm	J_{ER}	$5 \times 10^{-14}A/cm^2$
S_{CD}	4 μm	m	1.92
L_e	50 pH	C_{pbe}	0.11 fF
L_b	0.47 pH	C_{pce}	0.10 fF
L_c	0.29 pH	C_{pbc}	9.4 fF

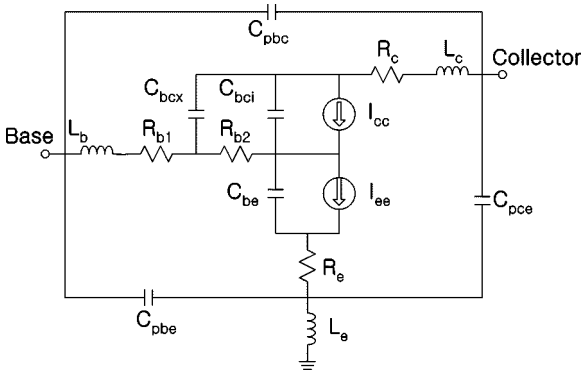

Fig. 2. HBT large-signal model.

the base and collector are S_{EB} and S_{BC}, respectively. The device model parameters used in the simulation are summarized in Table I. All equivalent-circuit parameter values are obtained as functions of the HBT structures [13], [14].

Fig. 2 shows the nonlinear equivalent circuit for the analysis. In the figure, R_e, R_{b1}, and R_{b2} are linear components while R_c, I_{ee}, I_{cc}, C_{be}, C_{bci}, and C_{bcx} are bias-dependent nonlinear components, which are calculated from the HBT structure. L_e, L_b, L_c, C_{pbc}, C_{pce}, and C_{pbe} are parasitics and are extracted by fitting to the measured s-parameter data. The parasitics for our devices are also listed in Table I. The ohmic resistances of the HBT are calculated from the following equations:

$$R_e = \frac{\rho_{EC}}{S_E L_E} + \frac{1}{q\mu_{nE} N_E} \frac{W_E}{S_E L_E} \tag{1}$$

$$R_{b1} = \frac{R_{SB} S_{EB}}{2L_E} + \frac{\sqrt{\rho_{BC} R_{SB}}}{2L_B} \coth S_B \sqrt{\frac{R_{SB}}{\rho_{BC}}} \tag{2}$$

$$R_{b2} = \frac{R_{SB} S_E}{12 L_E} \tag{3}$$

$$R_c = \frac{R_{SC} S_{CD}}{12 L_C} + \frac{\sqrt{\rho_{CC} R_{SC}}}{2L_C} \coth S_C \sqrt{\frac{R_{SC}}{\rho_{CC}}} + \frac{R_{SC} S_{BC}}{2L_C} + \frac{1}{q\mu_{nC} N_C} \frac{W_C - X_C}{S_{CD} L_C} \tag{4}$$

where ρ_{EC}, ρ_{BC}, and ρ_{CC} are the specific contact resistivities of the emitter, base, and collector, respectively, while R_{SB}, and R_{SC} are the sheet resistances of the base and subcollector layers, respectively, and X_C is the thickness of the depleted collector. All the other parameters have their nominal meanings.

The nonlinear current sources I_{ee} and I_{cc} are given by [14]

$$I_{ee} = I_{ES}\left[\exp\frac{qV_{be}}{kT} - 1\right] - \alpha_I I_{CS}\left[\exp\frac{qV_{bc}}{kT} - 1\right] + I_{ER}\left[\exp\frac{qV_{be}}{mkT} - 1\right] \tag{5}$$

$$I_{cc} = \alpha_F I_{ES}\left[\exp\frac{qV_{be}}{kT} - 1\right] - I_{CS}\left[\exp\frac{qV_{bc}}{kT} - 1\right] \tag{6}$$

where I_{ES}, α_F, I_{CS}, and α_I represent the emitter saturation current and current transfer ratio in the normal mode and the collector saturation current and current transfer ratio in the inverted mode, respectively, and I_{ER} accounts for the recombination current.

The stored charges at the base–emitter junction Q_{be} are composed of depletion and diffusion charges and are given by

$$Q_{be} = \sqrt{2\epsilon q N_E}\left(\sqrt{\phi_{be}} - \sqrt{\phi_{be} - V_{be}}\right) A_E + I_{ee}\tau_B \tag{7}$$

where τ_B is the base transit time. The base–emitter capacitance can be calculated from (dQ_{be}/dV_{be}) in the ADS program.

The C_{bci} is carefully modeled. The model includes the effect of the ionized donor charge in the collector-depleted region, which was compensated by the injected mobile charge. The depletion thickness (X_C) in the collector is modulated by the injection charges [15], and even for the device with an undepleted collector at a given collector bias, the collector can be fully depleted by the charge. Assuming that the conduction current in the collector region is mostly by drift and the carriers travel at a constant velocity of $v_{\rm sat}$, the mobile carrier concentration in the base–collector junction is simply $n = J_C/qv_{\rm sat}$, where J_C is collector current density. The Poisson equation in the depleted collector region simplifies to

$$\frac{d\varepsilon}{dx} = \frac{1}{\epsilon_s}\left(qN_C - \frac{J_C}{v_{\rm sat}}\right). \tag{8}$$

By integration of both sides for the depletion region from $x = 0$ to X_C with the boundary condition of electric field $\varepsilon(X_C) = 0$, we obtain

$$\varepsilon(x) = \frac{1}{\epsilon_s}\left(qN_C - \frac{J_C}{v_{\rm sat}}\right)(x - X_C). \tag{9}$$

We obtain the potential by integrating one more time from $x = 0$ to X_C as follows:

$$V_{cbj} + \phi_{cb} = \frac{1}{\epsilon_s}\left(qN_C - \frac{J_C}{v_{\rm sat}}\right)\frac{X_C^2}{2}. \tag{10}$$

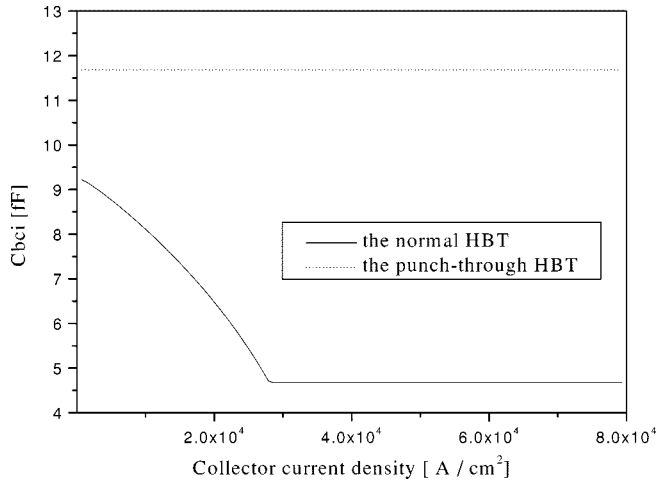

Fig. 3. Collector current dependency of C_{bci} at $V_{CE} = 3.5$ V for the normal HBT and the punch-through HBT.

Here, ϕ_{cb} represents the built-in potential. The junction voltage is equal to the applied base–collector bias (V_{cb}) minus the resistive voltage drop in the undepleted collector layer as follows:

$$V_{cbj} = V_{cb} - J_C \rho_C (W_C - X_C) \tag{11}$$

where ρ_C is the resistivity of the undepleted collector layer. The depletion thickness X_C is dependent on J_C and V_{BC} and is given by (12), shown at the bottom of this page, where $J_1 = qv_{\rm sat}N_C$. This equation is applicable for the collector current density J_C smaller than J_1. The charge at the intrinsic region of the base–collector junction Q_{bci} is given by

$$Q_{bci} = A_E X_C \left(qN_C - \frac{J_C}{v_{\rm sat}} \right). \tag{13}$$

C_{bci} is, therefore, dependent not only on the base–collector voltage, but also on the collector current. The intrinsic base–collector capacitor C_{bci} is obtained from (dQ_{bci}/dV_{bc}) routine of ADS. The current-dependent C_{bci} at the bias voltage $V_{CE} = 3.5$ V is extracted from the model and is depicted in Fig. 3. The C_{bci} of the punch-through HBT is constant for the all collector current levels. The C_{bci} of normal HBT is, however, dependent on the collector current density. As the collector current increases, the depleted region thickens and C_{bci} becomes smaller. At a higher current density (above 28 kA/cm^2), the collector is fully depleted, and C_{bci} becomes constant.

It can be assumed that the injected electrons seldom enter the extrinsic collector area [15]. The compensation effects by the mobile charge is negligible in the extrinsic collector region. The depletion thickness (X_{CX}) in the extrinsic region and extrinsic base–collector capacitance C_{bcx} are modeled as

$$X_{CX} = \sqrt{\frac{2\epsilon_s(\phi_{bi} + V_{cb})}{qN_C}} \tag{14}$$

$$\begin{aligned} C_{bcx} &= \frac{\epsilon_s(A_C - A_E)}{X_{CX}}, \qquad \text{for } X_{CX} \le W_C \\ &= \frac{\epsilon_s(A_C - A_E)}{W_C}, \qquad \text{for } X_{CX} > W_C. \end{aligned} \tag{15}$$

Self-heating effects are also considered [16]. The Kirk current density of the GaAs-based HBT is much higher than Si bipolar junction transistors (BJTs) [17]–[19], and the base push out has not been observed within the bias range of our measurement.

III. Experimental Results

We fabricated AlGaAs/GaAs HBTs using the self-aligned base metal (SABM) process with mesa isolation. The AlGaAs/GaAs HBT epi structure grown by MOCVD consists of an n+-InGaAs cap layer, an n-GaAs layer, an n-AlGaAs emitter layer, a C-doped p+-GaAs base layer, an n-GaAs collector layer, and an n+-GaAs sub-collector layer. The HBTs with punch-through collector and normal collector have the same structures, except for their collector thicknesses. The HBT with the punch-through structure has a 0.4-μm-thick collector doped to 2×10^{16} cm^{-3} and the other has a 1.0-μm-thick collector with the same doping. A thick gold metal layer was deposited on the emitter to improve the electrical and thermal performances. We also used the emitter widening process using polyimide. A substrate was lapped to the thickness of 100 μm and an emitter is grounded with a via hole. We have built several sized HBTs and Fig. 4 shows the photograph of the fabricated power HBT, which has 32 emitter fingers with a size of 2 μm $\times$ 22 μm.

Fig. 5 shows the measured and simulated $I_C - V_{CE}$ characteristics for the HBT with a single 2 μm $\times$ 22 μm emitter. The maximum current gains of both HBTs are about 30. The breakdown voltage at an open base BV_{ceo} is 10 V for the punch-through collector and 17 V for the normal one. Microwave performances of the fabricated HBTs are shown in Fig. 6. The f_T and $f_{\rm max}$ are 70 and 80 GHz, respectively, at $I_C = 18$ mA and $V_{CE} = 2.0$ V for the punch-through collector structure, and 55 and 125 GHz, respectively, at $I_C = 16$ mA and $V_{CE} = 2.3$ V for the normal collector structure. Fig. 7 illustrates the calculated and measured HBT s-parameter characteristics. Considering the physical model, a good agreement exists between the present model and measured dc and s-parameter data.

$$X_C = \frac{\epsilon_s \rho_C J_C}{qN_C}\left(1 - \frac{J_C}{J_1}\right)^{-1} + \sqrt{\left(\frac{\epsilon_s \rho_C J_C}{qN_C}\right)^2 \left(1 - \frac{J_C}{J_1}\right)^{-2} + \frac{2\epsilon(V_{cb} + \phi_{bi})}{qN_C}\left(1 - \frac{J_C}{J_1}\right)^{-1} - \frac{2\epsilon_s \rho_C J_C W_C}{qN_C}\left(1 - \frac{J_C}{J_1}\right)^{-1}} \tag{12}$$

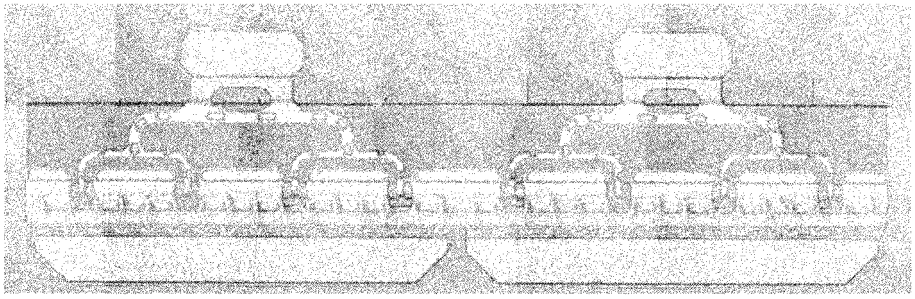

Fig. 4. AlGaAs/GaAs HBT with 32 × 2 μm × 22 μm emitters.

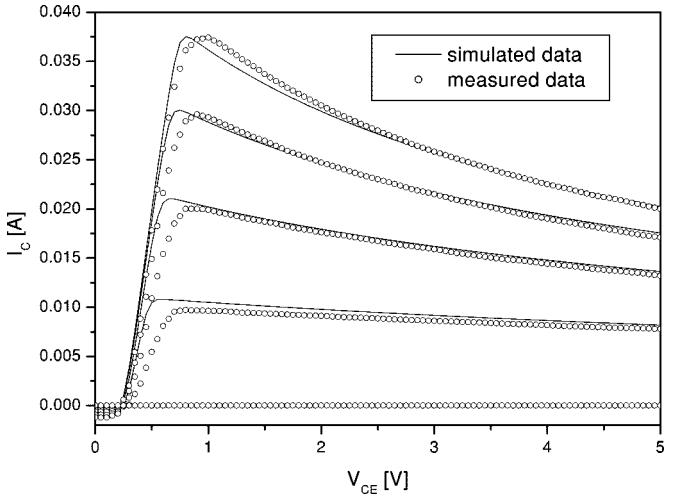

Fig. 5. Simulated and measured $I_C - V_{CE}$ characteristics of a 2 × 22 μm^2 AlGaAsGaAs HBT. The base current is 0.3 mA per step.

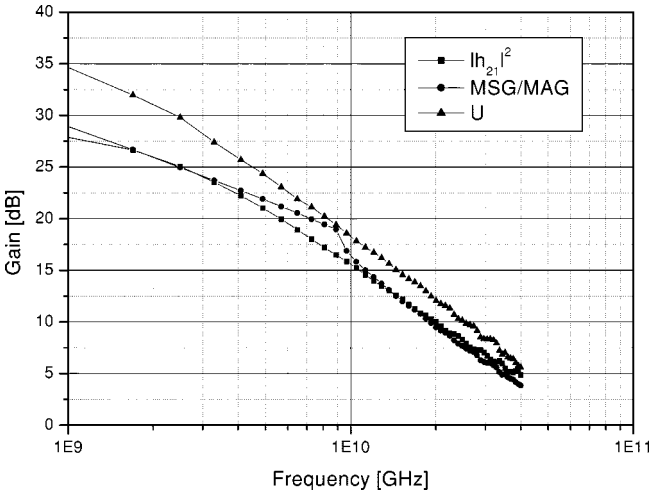

(a)

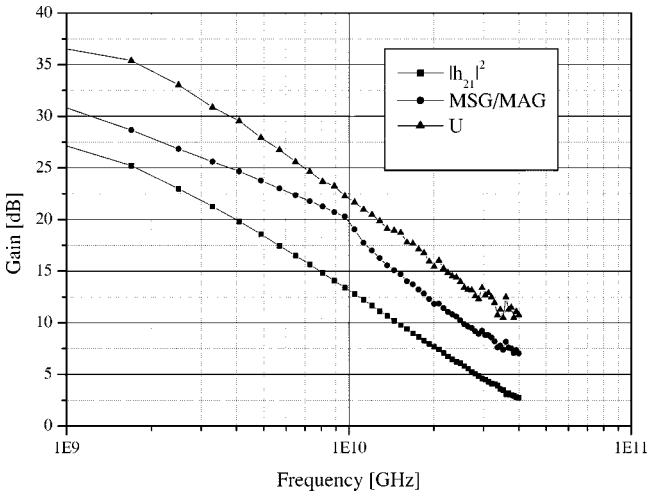

(b)

Fig. 6. Frequency dependence of $|h_{21}|^2$, maximum stable gain (MSG)/ maximum available gain (MAG), and unilateral gain (U) as determined by s-parameter measurements. (a) HBT with punch-through collector. (b) HBT with normal collector.

The power test results at 2 GHz for the 32-emitter finger HBTs are illustrated in Fig. 8, together with the two-tone test results. The dc-bias point is $I_C = 350$ mA and $V_{CE} = 3.5$ V. The punch-through HBT and the normal one exhibit a power gain of 16.6 and 16.9 dB, respectively, with output power of 28.9 and 28.6 dBm, respectively, and power-added efficiency (PAE) of 51% and 59%, respectively, at a 1-dB gain compression point. The source and load pulls using an automatic tuner are performed to locate the matching points for maximum gain and output power. Input matching impedances for the punch-through device and the normal one are 5.24-j1.05 and 4.74-j1.51, respectively. Output matching impedances are 6.33-j2.70 and 5.61-j7.87, respectively.

A two-tone test is carried out at 2 GHz. Two-tone spacing is 1 MHz to reduce the thermal effects on the linearity of AlGaAs/GaAs [20]. The matching points and bias conditions for the two HBTs are the same as the power test. Their IM3 distortion behaviors are remarkably different, as seen in Fig. 8. At a low input power, the HBT with the punch-through collector has a much lower IM3 than the normal HBT. The IP3 difference is 14.8 dB (39.5 versus 24.7 dBm). As the input power level increases (in our case, above −8.26 dBm), the IM3 of the normal HBT grows at a much slower pace than the normal 3 : 1 slope. However, at a large input power, the slope again increases at a ratio larger than 3 : 1, and in this region, the IM3 distortion of the both HBTs are comparable.

IV. Analytical Study

To understand the IM3 behaviors of the two HBTs, harmonic balance simulations were performed at 2 GHz for both structure HBTs with a 32–finger emitter. The operation conditions, bias points, and matching impedances were set at the same values of the measurement case. Fig. 9 shows the simulation results and

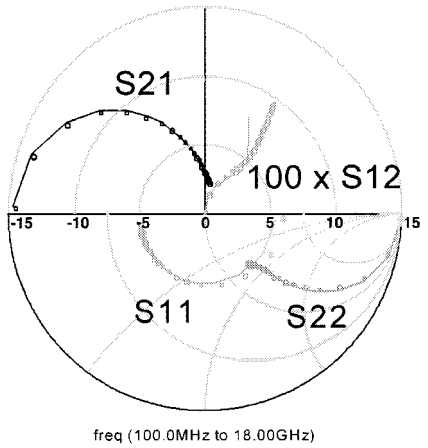

Fig. 7. Comparison of s-parameters from the model and measurement. The lines are simulated data and circles are measured data.

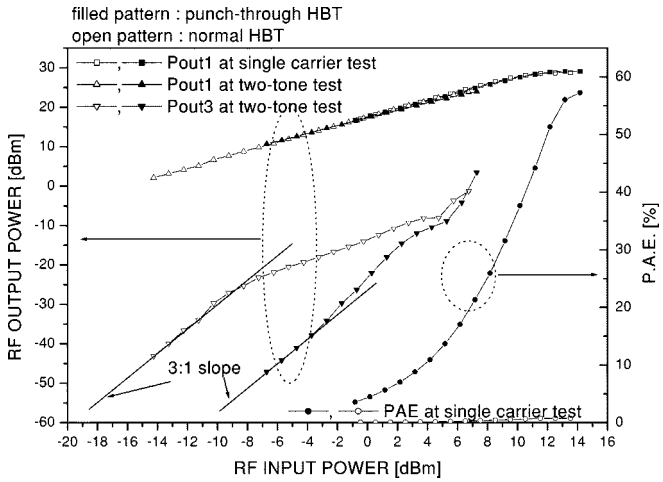

Fig. 8. Single- and two-tone test results of the fabricated power HBTs.

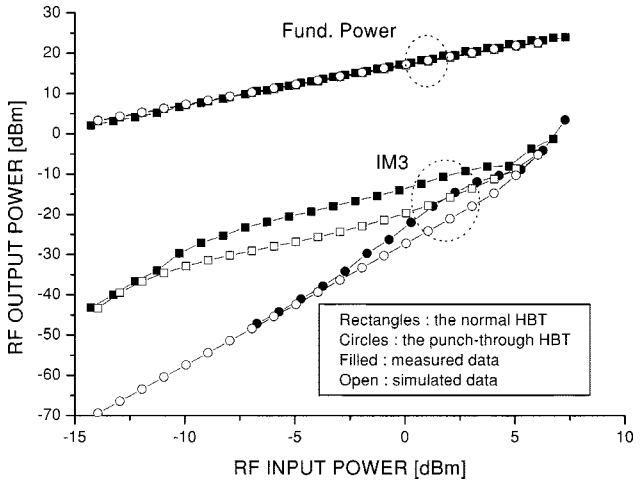

Fig. 9. Simulation results of the output power and its IM3 for the 32-finger HBTs. For comparison, the measured data are also included.

a reasonable agreement between the measured and simulated data. Our model indicates that the IM3 of the punch-through HBT is generated by the g_m nonlinearity, since the collector

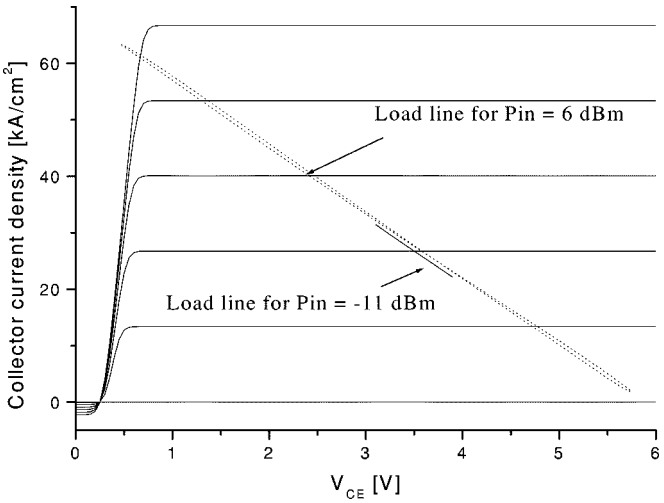

Fig. 10. Simulated $J_C - V_{CE}$ characteristics as seen by the RF signal and the load lines with -11 and 6 dBm, respectively, of the input power.

is fully depleted and C_{bci} is constant for all power levels. The IM3 follows the 3 : 1 gain slope reasonably well. The origin of the different IM3 characteristics of the two HBTs is C_{bci} since our physical models are exactly identical (except the C_{bci} of the charge modulated collector depletion layer). To understand the C_{bci} effect, the input power-dependent RF collector current swing is calculated using the load-line concept. Fig. 10 shows simulated $J_C - V_{CE}$ characteristics as seen by the RF signal and the load lines with -11 and 6 dBm of input powers. The collector current density at the bias point is 26 kA/cm^2 and the collector region is not fully depleted (see Fig. 3). At a small-signal level (in our case, below -11 dBm), the load line sees the nonlinearity of C_{bci} near the bias point and the IM3 has the normal 3 : 1 gain slope, but is a much higher level than the punch-through HBT. The load line at $P_{\rm in} = -11$ dBm moves on between 22–31 kA/cm^2 of J_C. Considering the reduced RF collector voltage at a high current level, the collector is fully depleted at the current density of 31 kA/cm^2. Therefore, for the input power above -11 dBm, the portion of the load line passes through the constant C_{bci} region and the growth rate of the IM3 starts to decrease (see Fig. 9). As the input signal increases further, a larger portion of the load line passes the region with constant C_{bci} and, finally, the IM3 is reduced to that of the punch-through HBT. Above 6 dBm of input, the load line touches the saturation region and very strong harmonics can be generated for both devices, and their IM3s are comparable.

V. Conclusion

The collector capacitance of an HBT is the dominant nonlinear element and the HBT with a punch-though collector is reported to have improved linear characteristics. To study the C_{bc} effect on the linearity, we have compared the properties of HBTs with a punch-through collector and a normal collector. For this purpose, we developed an analytical nonlinear HBT equivalent-circuit model. The present model includes the effect of the ionized charge in the depleted collector region compensated by the injected mobile charge. For the normal HBT, the IM can have a normal 3 : 1 gain slope at a small-signal range

because the load line moves in the region near to the bias point and sees the nonlinearity of C_{bci}. At a large-signal level, the load line passes through some region with a constant C_{bci} formed by the fully depleted collector, and the growth rate of IM3 is decreased. The punch-through HBT has a constant C_{bci} during the whole RF cycle, and its IM3 has the normal 3 : 1 gain slope for all input signal levels. Therefore, the IM3 level is lower for the punch-through collector HBT at a lower power level, but the IM3 of both devices are comparable at a high power level. To verify our simulation results, HBTs with a punch-through collector and normal collector were fabricated and tested. At a low-input signal, the HBT with a punch-through collector has much lower IM3 than does the normal HBT. The IP3 difference is 14.8 dB (39.5 versus 24.7 dBm). The differences are reduced as the power level increases, and around $P_{1\mathrm{dB}}$, the IM3 level of the two HBTs are quite comparable.

ACKNOWLEDGMENT

The authors would like to thank H. C. Seo, Eoncom Ltd., Sihenug, Kyonggido, Korea, for his assistance in the sawing process. The authors would also like to thank B. Ihn, Samsung Electronics Corporation Ltd., Yongin, Kyonggido, Korea, and D. S. Pang, Samsung Electronics Corporation Ltd., Yongin, Kyonggido, Korea, for their help for lapping process.

REFERENCES

[1] C. T. M. Chang and H.-T. Yuan, "GaAs HBT's for high-speed digital integrated circuit applications," *Proc. IEEE*, vol. 81, pp. 1727–1743, Dec. 1993.

[2] P. M. Asbeck, M. F. Chang, J. J. Corcoran, J. F. Jensen, R. N. Nottenburg, A. Oki, and H. T. Yuan, "HBT application prospects in the US: Where and when?," in *IEEE GaAs IC Tech. Symp. Dig.*, Monterey, CA, Oct. 1991, pp. 7–10.

[3] G.-B. Gao, D. J. Roulston, and H. Morkoc, "Design study of AlGaAs/GaAs HBTs," *IEEE Trans. Electron Devices*, vol. 37, pp. 1199–1208, May 1990.

[4] M. E. Kim, A. K. Oki, J. B. Camou, P. D. Chow, B. L. Nelson, D. M. Smith, J. C. Canyon, C. C. Yang, R. Dixit, and B. R. Allen, "12–40 GHz low harmonic distortion and phase noise performance of GaAs HBTs," in *IEEE GaAs IC Symp. Dig.*, Nov. 1988, pp. 117–120.

[5] S. A. Maas, B. L. Nelson, and D. L. Tait, "Intermodulations in HBTs," *IEEE Trans. Microwave Theory Tech.*, vol. 40, pp. 442–448, Mar. 1992.

[6] T. Iwai, S. Ohara, H. Yamada, Y. Yamaguchi, K. Imanishi, and K. Joshin, "High efficiency and high linearity InGaP/GaAs HBT power amplifiers: Matching techniques of source and load impedance to improve phase distortion and linearity," *IEEE Trans. Electron Devices*, vol. 45, pp. 1196–1200, June 1998.

[7] K. W. Kobayashi, J. C. Cowles, L. T. Tran, A. Gutierrez-Aitken, M. Nishimoto, J. H. Elliott, T. R. Block, A. K. Oki, and D. C. Streit, "A 44-GHz-high IP3 InP HBT MMIC amplifier for low DC power millimeter-wave receiver applications," *IEEE J. Solid-State Circuits*, vol. 34, pp. 1188–1194, Sept. 1999.

[8] A. Samelis and D. Pavlidis, "Mechanisms determining third order intermodulation distortion in AlGaAs/GaAs HBTs," *IEEE Trans. Microwave Theory Tech.*, vol. 40, pp. 2374–2380, Dec. 1992.

[9] N. L. Wang, W. J. Ho, and J. A. Higgins, "AlGaAs/GaAs HBT linearity characteristics," *IEEE Trans. Microwave Theory Tech.*, vol. 42, pp. 1845–1850, Oct. 1994.

[10] J. Lee, W. Kim, T. Rho, and B. Kim, "Intermodulation mechanism and linearization of AlGaAs/GaAs HBT's," *IEEE Trans. Microwave Theory Tech.*, vol. 45, pp. 2065–2072, Dec. 1997.

[11] P. Asbeck, "HBT linearity and basic linearization approaches," presented at the IEEE MTT-S Int. Microwave Symp. Workshop, Baltimore, MD, June 1998.

[12] M. Iwamoto, T. S. Low, C. P. Hutchinson, J. B. Scott, A. Cognata, X. Qin, L. H. Camnitz, P. M. Asbeck, and D. C. D'Avanzo, "Influence of collector design on InGaP/GaAs HBT linearity," in *IEEE MTT-S Int. Microwave Symp. Dig.*, Boston, MA, Jun. 2000, pp. 757–760.

[13] H. C. Casey, Jr. and M. B. Panish, *Heterostructure Lasers*. New York: Academic, 1978.

[14] A. A. Grinberg, M. S. Shur, R. J. Fischer, and H. Morkoc, "An investigation of the effect of graded layers and tunneling on the performance of AlGaAs/GaAs HBTs," *IEEE Trans. Electron Devices*, vol. ED-31, pp. 1758–1765, Dec. 1984.

[15] W. Liu, *Handbook of III–V Heterojunction Bipolar Transistor*. New York: Wiley, 1998.

[16] J. J. Liou, L. L. Liou, C. I. Huang, and B. Bayraktaroglu, "A physics-based, analytical heterojunction bipolar transistor model including thermal and high-current effects," *IEEE Trans. Electron Devices*, vol. 40, pp. 1570–1577, Sept. 1993.

[17] C. T. Kirk Jr., "A theory of transistor cutoff frequency (f_T) falloff at high current densities," *IRE Trans. Electron Devices*, vol. ED-9, pp. 164–174, Mar. 1962.

[18] P. C. C. Grossman and J. Chroma Jr., "Large signal modeling of HBT's including self-heating and transit time effects," *IEEE Trans. Microwave Theory Tech.*, vol. 40, pp. 449–464, Mar. 1992.

[19] J. Lee, B. Kim, Y. Kim, and S. Park, "A comparative study of the kirk effect in GaAs and Si BJTs," *Solid State Electron.*, vol. 37, no. 8, pp. 1485–1490, 1994.

[20] K. Lu, P. M. McIntosh, C. M. Snowden, and R. D. Pollard, "Low-frequency dispersion and its influence on the intermodulation performance of AlGaAs/GaAs HBTs," in *IEEE MTT-S Int. Microwave Symp. Dig.*, San Francisco, CA, June 1996, pp. 1373–1376.

Woonyun Kim (S'95–M'01) was born in Seoul, Korea, in 1970. He received the B.S., M.S., and Ph.D. degrees in electronic and electrical engineering from the Pohang University of Science and Technology (POSTECH), Pohang, Korea, in 1994, 1996, and 2001, respectively.

His research interests include fabrication, modeling, and characterization of GaAs- and InP-based HBTs, especially the linearity of HBTs.

Sanghoon Kang was born in Pusan, Korea, in 1972. He received the B.S. and M.S. degrees in electrical engineering from the Pohang University of Science and Technology (POSTECH), Pohang, Korea, in 1996 and 1998, respectively, and is currently working toward the Ph.D. degree at POSTECH.

His research interests are front-ends radio-frequency integrated-circuit (RFIC) design, mixer linearity, and noise.

Kyungho Lee was born in Miryang, Korea, in 1975. He received the B.S. degree in electronics and electrical engineering from the Kyungpook National University, Taegu, Korea, in 1999, the M.S. degree in electronics and electrical engineering from the Pohang University of Science and Technology (POSTECH), Pohang, Korea, in 2001, and is currently working toward the Ph.D. degree at POSTECH.

His research interests are development of high-speed HBTs, including GaAs- and InP-based HBTs, and their applications.

Minchul Chung received the B.S. and M.S. degrees in electronic and electrical engineering from the Pohang University of Science and Technology (POSTECH), Pohang, Korea, in 1997 and 1999, respectively, and is currently working toward the Ph.D. degree at POSTECH.

His research interests are the design and fabrication of GaAs-based low noise HBTs and monolithic microwave integrated circuits (MMICs), including low phase-noise HBT oscillators.

Youngoo Yang (S'99) was born in Hamyang, Korea, in 1969. He received the B.S. degree in electronic engineering from the Han-Yang University, Ansan, Korea, and is currently working toward the Ph.D. degree at the Pohang University of Science and Technology (POSTECH), Pohang, Korea.

His research interests include linearization techniques, and behavioral modeling of high-power amplifiers, large-signal modeling of microwave devices, and RFIC design.

Bumman Kim (S'77–M'78–SM'97) received the Ph.D. degree in electrical engineering from Carnegie-Mellon University, Pittsburgh, PA, in 1979.

From 1978 to 1981, he was engaged in fiber-optic component research at GTE Laboratories Inc. In 1981, he joined the Central Research Laboratories, Texas Instruments Incorporated, where he was involved in development of GaAs power FETs and MMICs. He developed a large-signal model of a power FET, dual-gate FETs for gain control, high-power distributed amplifiers, and various millimeter-wave MMICs. In 1989, he joined the Pohang University of Science and Technology (POSTECH), Pohang, Korea, where he is currently a Professor in the Electronic and Electrical Engineering Department, and Director of the Microwave Application Research Center, where he is involved with device and circuit technology for MMICs. He has authored or co-authored over 100 technical papers in this area.

Dr. Kim is a member of the Korean Academy of Science and Technology.